Evaluation of Fade-Recovery Performance of Hybrid Friction Composites Based on Ternary Combination of Ceramic-Fibers, Ceramic-Whiskers, and Aramid-Fibers

Mukesh Kumar,[1] Bhabani K. Satapathy,[2] Amar Patnaik,[1] Dilip K. Kolluri,[3] Bharat S. Tomar[4]

[1]*Department of Mechanical Engineering, N.I.T Hamirpur, Himachal Pradesh-177005, India*
[2]*Centre for Polymer Science and Engineering, I.I.T Delhi, New Delhi-110016, India*
[3]*Tribology Laboratory, 50 Nanyang Avenue, N3.1-B3b-03, 639798, Singapore*
[4]*Allied Nippon Industries, Sahibabad, Uttar Pradesh, India*

Received 11 April 2011; accepted 26 August 2011
DOI 10.1002/app.35550
Published online 22 November 2011 in Wiley Online Library (wileyonlinelibrary.com).

ABSTRACT: Hybrid composite friction material based on ternary combination of potassium titanate whiskers, alumino-silicate ceramic fibers, and aramid fibers were fabricated and evaluated for their physical, mechanical, and tribo-performance. The frictional response, friction-fade, friction-recovery, and wear properties have been characterized on a Krauss friction tester following ECE R-90 regulation. Optimally, the composite with hybrid reinforcement incorporations in the form of ceramic-whiskers, ceramic-fiber, and aramid-fiber in the ratio of 13.75 : 13.75 : 2.5 has potentially been explored as a functionally feasible friction-material for braking applications. The interdependence of fade, recovery, disc temperature rise, and wear characteristics is established via thematic correlation diagram. © 2011 Wiley Periodicals, Inc. J Appl Polym Sci 124: 3650–3661, 2012

Key words: composites; mechanical properties; reinforcements

INTRODUCTION

Continuous emphasis on the development of durable and efficient friction materials for braking applications conforming to the stringent norms, such as, higher friction coefficient, negligible fading, faster recovery, better wear resistance, low-sensitivity towards load-speed alterations, least noise, and vibration propensity for safe and reliable operation over a wider range of braking applications has been the theme of automotive braking industries. Conventionally, these heterogeneous composites are consisting primarily of four classes of ingredients binder, fibers, fillers, and friction modifiers. The crucial contribution of fibers in enhancing physical, mechanical, and tribo-performance (like wear stabilization/minimization and friction optimization) under the dynamic sets of operating variables is very well recognized.[1–9] The role of fiber-combinations based on inorganic-organic such as aramid-processed rock fiber (Lapinus^{TM}), polyacrylonitrile (PAN)-basalt volcanic rock fiber, aramid-basalt, cellulose-lapinus, carbon-lapinus, etc. and fibers combination based on organic-ceramic combinations such as aramid-potassium titanate, aramid-glass, etc. have been extensively studied.[10–27]

Kim et al.[17,18] reported that both aramid and potassium titanate whiskers have synergistic combination due to strong electrostatic attraction developed during mixing. Consequently, the friction film leads to a more stable friction coefficient (μ) and improves the wear resistance. Cho et al.[19] studied morphological effect of potassium titanate fibers on the tribological properties in braking situations and have reported the effect of whiskers on the overall performance of friction materials. Kumar et al.[28] studied binary combination of potassium titanate whiskers and aramid fiber with a whiskers-to-organic fiber ratio of = 5 : 1 where the composites reported showed higher friction-braking effectiveness. As ceramic fibers such as calcium-silicate fibers or alumino-silicate based fibers are known for their unique thermal resilience and inherent hardness[23,24] they have repeatedly been incorporated in many industrial brake material formulations. Patnaik et al.[29] studied binary combination of alumino-silicate ceramic fiber and aramid fiber and the fiber combination with a ceramic-to-organic fiber ratio of = 5 : 1 leading to an optimized overall performance.

In light of the above literatures, this investigation aims to explore the possible ternary combination of ceramic whiskers, ceramic fibers, and aramid fibers,

Correspondence to: A. Patnaik (amar_mech@sify.com).

TABLE I
Design of the Formulation

Ingredients (wt %)	Composite Nomenclatures				
	TSC-1	TSC-2	TSC-3	TSC-4	TSC-5
Phenolic resin	15	15	15	15	15
Barite ($BaSO_4$)	50	50	50	50	50
Graphite	5	5	5	5	5
Potassium titanate whiskers (PTW)	15	13.75	12.5	11.25	10
Alumino-silicate ceramic fibers	15	13.75	12.5	11.25	10
Aramid fibers	0	2.5	5	7.5	10

namely, potassium titanate whiskers, alumino-silicate ceramic fiber, and aramid fiber. The focus of the work is to establish a possible correlation between the composition and performance-attributes specifically with regard to enhanced frictional response, fade resistance, and faster recovery performance with promising wear reduction for the automotive braking application.

EXPERIMENTAL DETAILS

Fabrication of the friction composites

Straight phenolic resin (JA-10, binder), barite (inert filler), graphite (SK-304, S.K. Carbon Limited, India, lubricant) reinforced with aramid/Kevlar pulp (IF-258; Twaron, Teijin-Germany), potassium titanate whiskers (PTW; locally supplied by Jayesh Industries, India), and ceramic fiber (SM-70, Standard grade alumino-silicate fiber; M/s Murugappan-Morgan, India) amounting to 100% by weight are mixed and composites were fabricated as per designed formulations detailed in Table I and the processing conditions mentioned in Table II. To achieve mechanical isotropy while mixing, plough shear mixer is used. The molding conditions are adopted as per the standard industrial practice (i.e., keeping 10°C higher in the platens than the actual curing temperature i.e., 153°C as determined from DSC to compensate any heat/thermal losses via the mold/pattern to the atmosphere) depending on the curing isotherm of the matrix novolac resin. The adhesive coated back-plates of mild steel support the mold cavity (Fig. 1). Moisture and other gaseous by-products (because of polycondensation of the phenolic resin) during curing are allowed to expel via multiple intermittent breathings to prevent cracking of the composites. Finally, the pads are post cured (in muffle-furnace) to relieve the frozen-in stresses. The obtained composite pads are subjected to surface polishing under identical conditions prior to engaging them into tribological performance assessment following the adopted protocol. The same pads were characterized for various physical, mechanical, and tribo-properties.[28,29]

Physical, mechanical, and surface characterization

The physical and mechanical characterization of the polished friction composite samples such as their density, ash content, void fraction, hardness, shear strength, compressibility, tensile, flexural, and impact strength are presented in Table III. To confirm uniform mixing and proper curing during manufacturing the distribution of surface hardness is measured. The mechanical properties such as hardness (measures of extent of cross linking/curing, material resistance to indentation under load as an indirect measure of mechanical isotropy achieved due to mixing of the ingredients), cross breaking/shear strength (measures composite integrity throughout the bulk and adhesion with the back plate), compressibility (measures change in thickness under elastic or standard load during the test), tensile strength, flexural strength, and impact strength characteristics have been determined following the standards conforming to the industrial practice. The ash content is determined by roasting at a very high-temperature (≈840°C) for ~ 4 h in the muffle furnace following gravimetric methods. Hardness is measured on Rockwell hardness tester (Model TRS, S.No: 98/575) from Fine Testing Machine on the scale Rockwell A as per ASTM D785-65. The shear

TABLE II
Details of the Fabrication Conditions of the Composites

Procedure	Conditions
Mixer run and ingredients mixing sequence	Plough shear mixer with feeder at 150 rpm and chopper at 3000 rpm. First aramid pulp, potassium titanate whiskers (PTW), ceramic fibers (lighter in weight), and barite (heavier then fibers) are mixed for 5 min then other powdery ingredients are added for another 10 min. Thus, total mixing run is of 15 min
Compression molding machine setting	Curing temperature = 153°C (obtained from DSC curve) for 15 min at 15 MPa with three intermittent breathings
Post Curing setting	Post curing temperature: 170°C; 5 h
Finishing step	Lightly polished with grinding wheel (Carborundum Universal limited, GC 60, K5, V0) to attain the desired thickness (~ 15.34 mm) and to remove the glazed skin of binder from the surface

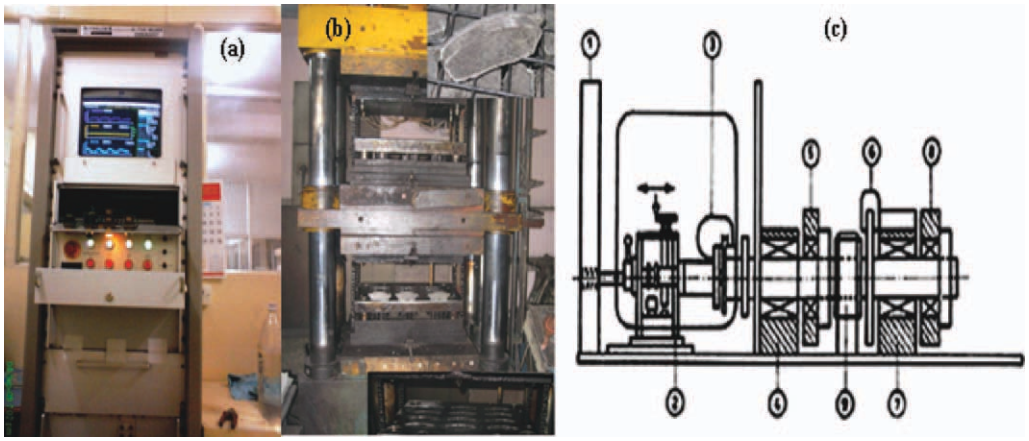

Figure 1 (a) Krauss friction testing machine: Computer interfaced data acquisition system [Automatic measuring equipment and test bencher, D-T141 MURR Germany]. (b) Compression molding machine (inserts) brake-pad and 12-cavity mold. (c) Schematic of Krauss test rig tribo-performance evaluation of brake pads (1) compressed air supply, (2) bearing movable, (3) air inlet, (4) bearings, (5) option SH 2.5 kg/m^2, (6) emergency stop option, (7) bearings, (8) options SH 5 kg/m^2, and (9) flywheels connected to DC motor housing through a belt drive with clutch option actuated by a generator.[28,29][Color figure can be viewed in the online issue, which is available at wileyonlinelibrary.com.]

strength is measured on universal testing machine (Model: UTN 20, S.No:9/83-603) from Fuel Instruments and Engineers, India. For compressibility test, Hind hydraulics compressibility testing machine was used, following ISO 6310 standards. Izod impact test is performed on (standard specimen size = 70 × 10 × 10 mm^3, 45° notch, and 2 mm deep at 47 mm clamped height in vice) pendulum impact tester (Model-IT 504) supplied by Tinius Olsen, England following ASTM D-256. For tensile test (specimen dimensions = 150 × 10 × 4 mm^3) and flexural test (specimen size = 60 × 10 × 4 mm^3; span length of 40 mm) universal testing machine of Hounsfield test equipment, England (Model No.: H2SK-SO 259) is used. It is interfaced with computer (DAS-RS 232 interface board) using QMat test generator software (for tensile test, test speed = 2.54 mm/min, gauge length = 55 mm, extension range = 25 mm, load range = 5 kN; for flexural test, test speed = 10 mm/min, extension range = 10 mm, span = 40 mm, and load range = 5 kN). The machine has force measuring resolution of 1/320,000 of load-cell capacity over the full range and accuracy of ±0.5% of indicated load from 2 to 100% of load-cell capacity. The theoretical density (ρ_{ct}) of the composite materials in terms of weight fraction can be obtained from[30]:

$$\rho_{ct} = \frac{1}{\frac{w_r}{\rho_r} + \frac{w_{f1}}{\rho_{f1}} + \frac{w_{f2}}{\rho_{f2}} + \frac{w_{f3}}{\rho_{f3}} + \frac{w_g}{\rho_g} + \frac{w_b}{\rho_b}} \quad (1)$$

where, w and ρ represent the weight fraction and density and the suffix *r, f1, f2 f3, g, and b* are corresponding to phenolic resin, potassium titanate whiskers, aramid fibers, alumino-silicate fiber, graphite, and barite. The actual density (ρ_{ca}) of the

TABLE III
Physical and Mechanical Properties of the Composites

Sample No. Properties	TSC-1 (15 : 15 : 1)[a]	TSC-2 (13.75 : 13.75 : 2.5)	TSC-3 (12.5 : 12.5 : 5)	TSC-4 (11.25 : 11.25 : 7.5)	TSC-5 (10 : 10 : 10)
Density (g/cc)	2.02	2.08	2.06	2.06	2.05
Ash content (%)	90	98	73	55	59
Hardness[b] (HR-R)	88.067	85.765	99.50	99.083	102.083
Shear load (Kgf) test	1180	1420	1220	1580	2040
Compressibility	0.66	0.69	0.49	0.36	0.49
Tensile strength (MPa)	9.40	7.77	13.45	7.14	12.57
Elongation (%)	1.31	4.93	3.07	1.70	3.15
Flexural strength (MPa)	44.71	17.38	49.05	50.70	68.30
Impact Energy (J)	0.1515	0.0566	0.2304	0.3194	0.2540
Impact strength (kJ/m^2)	0.20209	0.07557	0.30726	0.42586	0.33871
Void fraction (%)	9.9	13.7	14.6	16.6	17.9
Acetone extractable (mg)	0.0105	0.1072	0.0088	0.0082	0.0094

[a] 15 : 15 : 1 means proportions of (PTW : Alumino-silicate ceramic fiber : Aramid fiber).
[b] Averaged over 12 different points on the composite surface.

composite is determined by standard water immersion method following ASTM D792. The volume fraction of voids in the composites is calculated using the equation,

$$V_0 = \frac{\rho_{ct} - \rho_{ca}}{\rho_{ct}} \quad (2)$$

Scanning electron microscopy (SEM) was carried out on JSM-6100 apparatus from JEOL operating at 35 kV to analyze the associated wear mechanisms and structural integrity of such multiphase hybrid composite friction materials. The surface of the specimens was gold sputter coated prior to the examination to make the surface conductive using JFC-1100 fine coat ion sputter from JEOL.

Tribological performance evaluation method

The fade and recovery test were carried out on a fully computer-controlled Krauss type (RWDC) 100°C (450 V/50 Hz) tribo-machine with data acquisition capability. The machine can potentially generate inertia of 2.5 kg/m^2 at a rotational speed of 660 rpm. A pair of brake pads (total area of 30 cm^2) was put to braking engagement-disengagement via an actuated caliper assembly. The rotor disc (diameter of 215 mm, thickness 10.5 mm, and Brinell hardness of 183-212) as the counterface made up of pearlitic cast iron has a mean contact radius of 95 mm and the applied load on the brake pads was manipulated to a contact pressure of 2 MPa. The friction force and the temperatures of the disc were measured after every cycle/run of braking in a synchronized manner by using a load-cell and thermocouples touching along the circumference of the disc, respectively. The performance of the composite friction materials were evaluated for their cold-fade-recovery performance following the standard protocol PVW-3212 as per ECE R-90 (European Commission for Energy Reguation-90).

Procedure for standard test as per ECE R-90

The standard regulatory test protocol R-90 conforming to ECE (Economic Commission for Europe) has been adopted for the evaluation of cold friction-fade-recovery characteristics of the friction material. The protocol offers provisions for the approval of replacement of brake lining assemblies for the power driven vehicles and their trailers.[31] The procedure consists of two major parts, namely, bedding cycle and the actual friction assessment test cycles. To ensure more than 80% conformal contact bedding cycle was carried out. In the bedding runs, the polished pad surface is allowed to slide against the rotor disc for the initial 30 brakings of 10 s each under the normal braking pressure/load of 2 MPa and the speed of the rotor disc maintained at 660 rpm in such a manner that the temperature rise of the disc does not exceed 280°C. In case temperature exceeds the limit, it was brought to cool down to 100°C intermittently using air blower. Thus, mechanistically, bedding cycle ensures controlled friction induced thermal history, and avoids green fade. Then, the post bedding cycle, that is, the actual testing cycles resumes. The friction assessment test cycles consists of seven cycles/runs, namely, one cold run, five fade runs, and one recovery run. Each run is of 10 brakings with 10 s as the braking duration making the total number of braking operations in the entire test run 70. In cold friction run, initial temperature was maintained at 45°C. This follows five runs of fade termed as first, second, third, fourth, and fifth fade. Each fade run begins with initial temperature of 100°C and it rises uninterruptedly until the completion of the runs. The subsequent fade runs were carried out similarly. Finally, recovery run (7th cycle of the R-90 protocol) begins in which the disc was allowed to cool down to a temperature of 100°C aided by the air-blower. The friction force and the temperature rise of the disc surface are recorded after every cycle of the braking in a synchronized manner. The wear of the tribo-pairs, that is, disc and brake pad are measured in terms of change in the thickness and weight loss before and after the test.

RESULTS AND DISCUSSIONS

The various physical and mechanical properties of the fabricated composites are shown in the Table III. Figure 2(a–e) shows the frictional response of the composites plotted synchronously with the braking instances and braking induced temperature rise of the disc obtained from the Krauss friction tester. The composition dependence of the evolution of the friction build-up, friction-peaking, and friction-decaying phenomena has been found to be largely influencing the magnitude of the frictional performance, of which a critical qualitative analysis may be made from Figure 3(a–g). Figure 4(a–e) shows the SEM micrographs to study the wear mechanisms and the dynamics of contact patch formation-deformation-destruction-reformation.

Physical and mechanical characteristics of the composite

The physical and mechanical characteristics of said friction composites are illustrated in Table III. The following salient observation could be made; the variation ($\sim$ 55–98%) in the ash content magnitude of the said composites decreases appreciably with

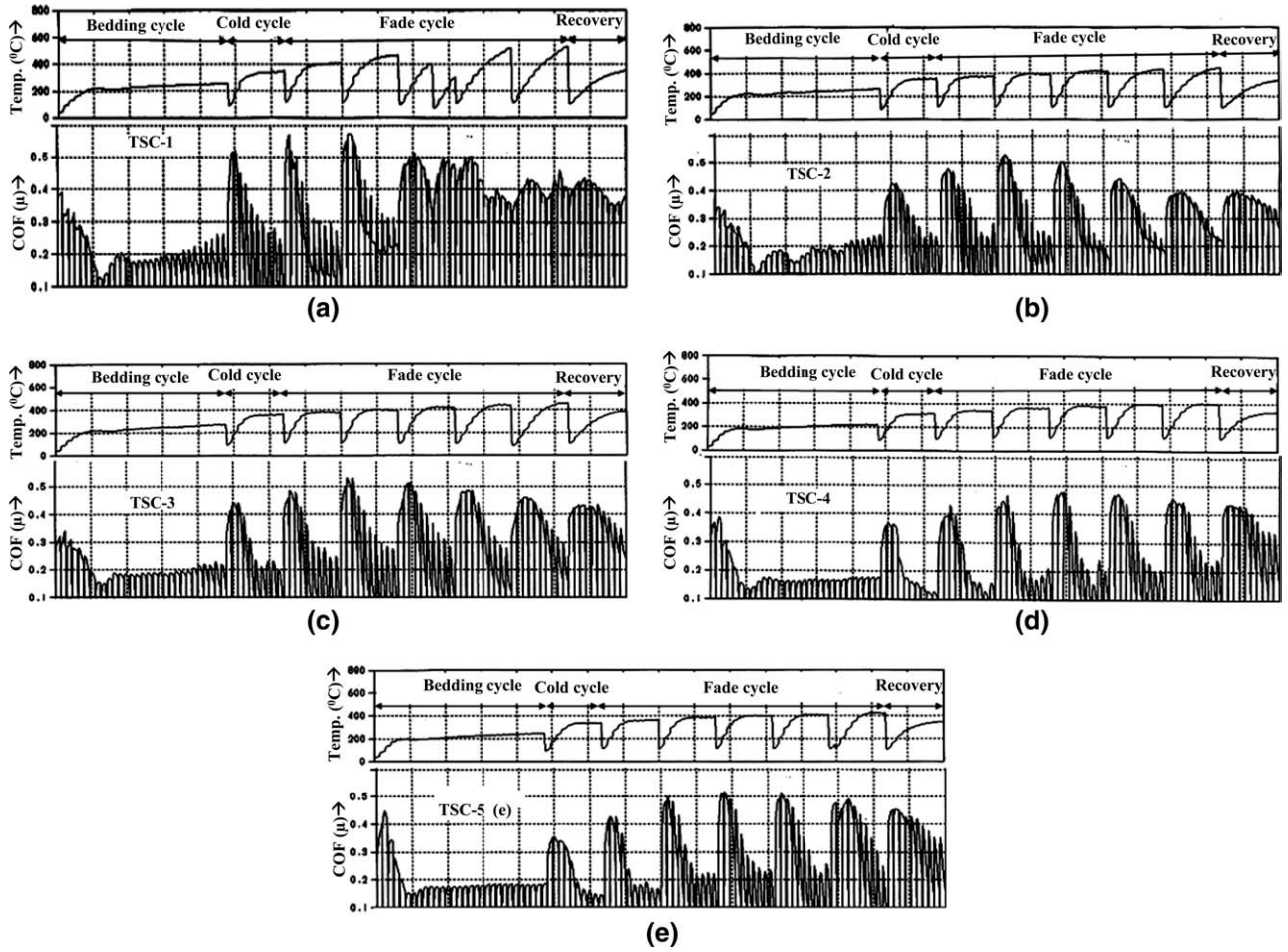

Figure 2 Frictional response of the composites plotted synchronously with the braking induced temperature rise of the disc (a) TSC-1, (b) TSC-2, (c) TSC-3, (d) TSC-4, and (e) TSC-5.

decrease in thermally stable ceramic fiber/whiskers complemented by organic fiber proportion. This attributed to roasting at higher temperature for several hours; the organic matter present in the friction composites finishes and leaving behind thermally stable ceramic fiber. Similarly, the compressibility variation (∼ 0.36–0.69%) follows similar trend may be attributed to influence of voids content; however, magnitude falls within the specified Industrial standard limits of 2%. The actual density of the composites remains appreciably similar (∼ 2.02–2.08 g/cc) with slight increase in magnitude with the compositional variations of the constituent's fibers. Similarly void fraction (∼ 9.9–17.9%), shear strength (∼ 1180–2040 MPa), flexural strength (∼ 17.38–68.3 MPa), impact energy (∼ 0.06–0.32 J)/impact strength (∼ 0.08–0.43 kJ/m^2), % elongation (1.3–4.93), and hardness (∼ 85.76–102.08 HR-R) characteristics of the said composites observed to follow similar increasing trend. The possible causes of increase in void fraction with composition variables are; the theoretical consideration for computation of density is based on idealistic assumption that differ experimentally evaluated density. Practically, lower density may be attributed to insufficient bonding at the interface of matrix and other ingredients that leave voids. The aggregation of microingredients because of electrical charge while mixing may create intraparticulate voids because of insufficient bonding with matrix. The possible error while fabrication may possibly results in voids. Its impractical to have zero void fraction; however, higher void fraction in composites are undesirable and represents inferior quality, as such composite material affects various properties and performance while in services.

The tensile strength (∼ 7.14–12.57 MPa) of the composites remains inappreciably affected by the compositional variations in the weight fraction of the constituent's fibers. The increase in the mechanical properties may attributed to the fact that increase in the aramid proportion increases the micro-packing of the fibers in the cured and crosslinked network of resin, that cause mechanical compaction of the fibrous ingredients thereby shows effective synergism, as has already been reported in Refs. 27–29. The role of fiber combinations to be influencing the

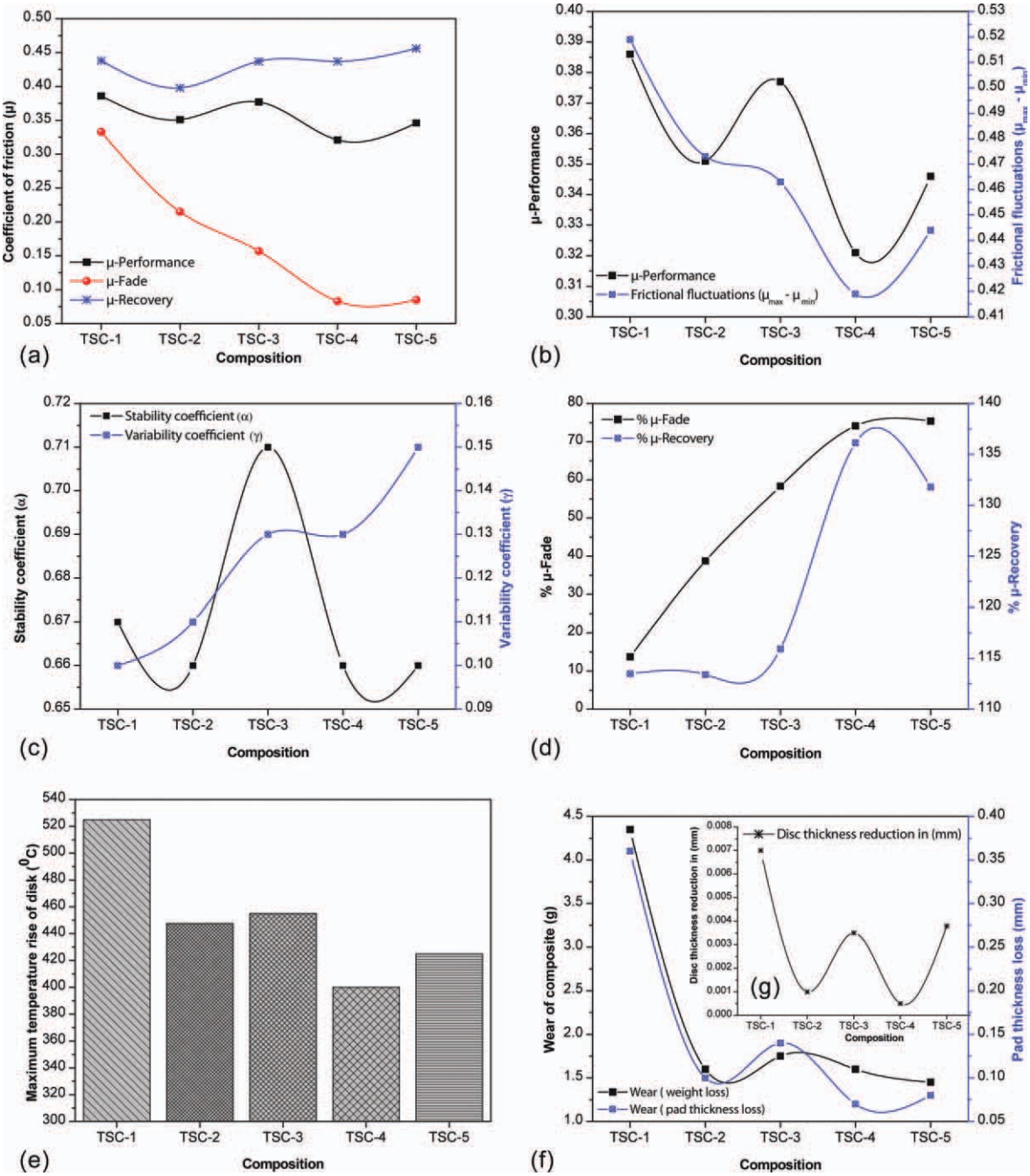

Figure 3 (a) Coefficient of friction (μ) of TSC-composites as a function of composition. (b) Friction performance [μ-performance (μp)] and frictional fluctuations ($\Delta\mu = \mu_{max} - \mu_{min}$) versus composition of the composites. (c) Stability coefficient (α) and Variability coefficient (γ) of TSC-composites as a function of composition. (d) Fade and recovery performance of TSC-composites as a function of composition. (e) Maximum temperature rise of disc (°C) versus composition of the composites. (f,g) Wear of composites and disc thickness reduction versus composition of the composites. [Color figure can be viewed in the online issue, which is available at wileyonlinelibrary.com.]

strength of the composites is well reported in literatures. The acetone extractable (∼ 0.0072–0.0105 mg) of the composites fairly increases as the proportion of organic content relative to ceramic content increases. It may attribute to net increase in organic content in resin matrix. The physical and mechanical properties of the investigated composites broadly remained within the range of industrial standards.

Friction characteristics of the composite

Frictional response of the composites

The synchronously plotted frictional response with the number of braking and the braking induced temperature rise of the disc are shown in Figure 2(a–e). The three regimes of friction evolution (viz., friction build-up, friction-peaking, and friction-decay stages)

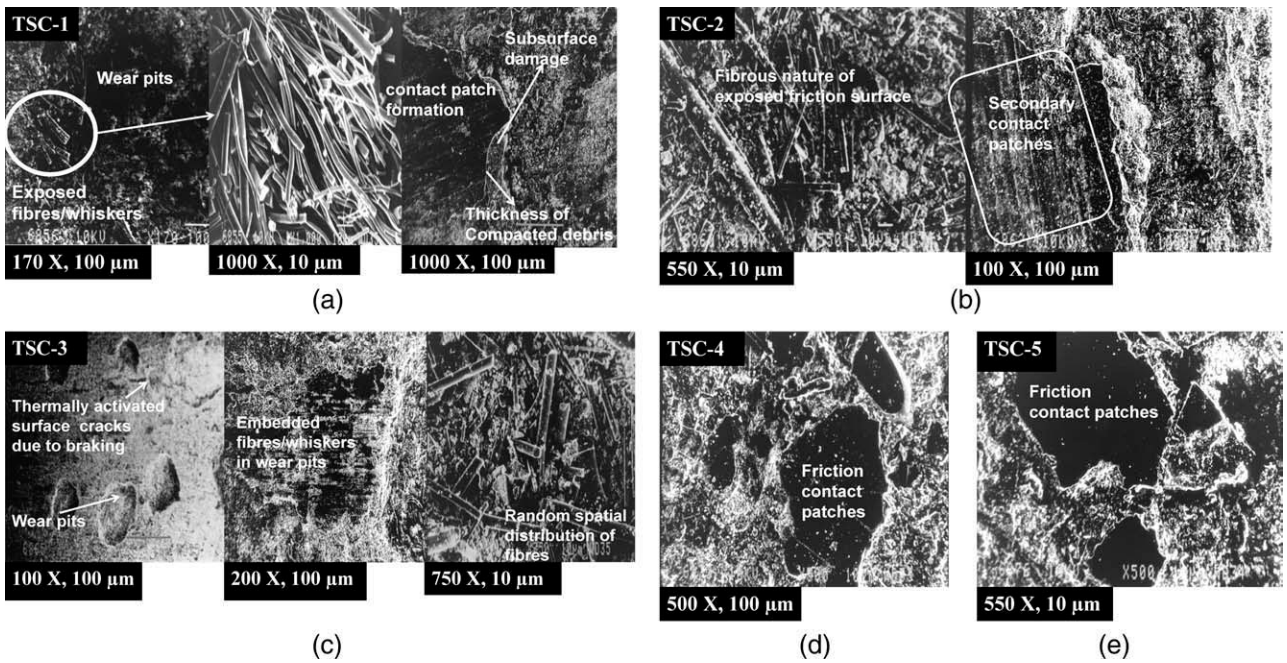

Figure 4 Wear micrograph (SEM) of TSC-composites (a) TSC-1, (b) TSC-2, (c) TSC-3, (d) TSC-4, and (e) TSC-5.

have been clearly demonstrated in the Figure 2 and the friction evolution characteristics remained independent of the composition and the test runs (viz., cold cycle run, fade runs, and recovery run). The friction build up process has been observed to be ensued in the early stages of cold and fade runs. However, during the later stages the friction-peaking and friction-decaying phenomenon was observed within a few braking instances irrespective of the compositions. The performance ideology from friction point of view may graphically be assumed like a perfect horizontal line parallel to *X*-axis (abscissa) with implications of a stable and high coefficient of friction.[28,29]

Friction performance of the composites

The observed friction coefficients lie broadly in the standard range of $\sim$ 0.3–0.5, which is acceptable for the light-duty motor vehicles[1] [Fig. 3(a)]. Further, it is observed that the composites having more ceramic fiber/whiskers (= 13.75 wt % each) and less aramid fiber (= 2.5 wt %), that is, TSC-1,TSC-2 showed promising friction coefficients combined with much less fading tendency under the low-inertia test conditions as in the Krauss friction tester whereas, other composites having less ceramic fiber/whiskers ($<$ 13.75 wt % each) and more aramid fiber ($>$ 2.5 wt %), that is, TSC-3, TSC-4, and TSC-5 showed comparatively larger magnitude of fade, that is, =58% under severe braking situation. This may be attributed to the dominant abrasion assisted wear mechanism aided by the predominantly ceramic nature of the operating friction film due to the combined presence of potassium titanate whiskers and aluminosilicate fibers in the composites. However, with the increase in aramid content the contribution from ceramic constituents gets reduced and thereby the surface friction film becomes increasingly organic leading to an enhanced susceptibility to thermal-degradation and shear-thinning at the braking interfaces. Therefore these composites exhibit poor fade resistance. It is well reported that friction film formation is largely influenced by mechano-chemical and surface energy interactions, due to variations in the nature of the disparate ingredients in the composites.[8]

The frictional-stability aspects has been analyzed by resorting to three quantitative parameters, that is, frictional fluctuations ($\Delta\mu = \mu_{max} - \mu_{min}$), stability coefficient (α) and variability coefficient (γ) and there correlation with the compositional variables is depicted in Figure 3(b,c). Theoretically, friction-stability as a key performance determinant is attributed to friction induced elastic and thermo-elastic fluctuations at the asperity junctions in the braking interface and across the operating friction films. Such composition induced friction fluctuations ($\mu_{max} - \mu_{min}$) have been observed to decrease systematically with the increase in aramid content indicating the friction film stabilization characteristics of aramid fiber. The compositions TSC-4 and TSC-5 showed the least frictional fluctuation since the adhesive component of friction optimally dominates the abrasive contribution due to a corresponding decrease in the ceramic whiskers/fiber contents. The

role of the abrasive component being aggravated in the other composites lead to higher friction assisted instabilities causing more intense fluctuations. Characteristically enhanced frictional fluctuations should always be minimized since they may promote noise and vibrations propensity.

Stability coefficient (α) measures response (stability/closeness) of magnitude of μ-performance with respect to μ-max. In general, moderate-to-high value is preferred for such a multiphased hybrid friction composites. The variations in the magnitude of μ-performance should be stable and close to that of μ-max for smooth frictional response while applying brakes, that is, to avoid judder, jerks, etc. However, variability coefficient (γ) measures response (variations) of magnitude of μ-min with respect to of μ-max. It should be least, to avoid real time brake failure due to loss of required friction coefficient while applying sudden brakes. The stability coefficient (α) of the composites showed moderate and comparable levels barring TSC-3 with strikingly higher stability whereas the variability coefficient (γ) showed an increasing trend with the increase in aramid fiber content, which may be due to shear thinning nature of the friction film. The composite having more ceramic whiskers/fiber content (=13.75 wt % each) in combination with less aramid fiber (=2.5 wt %) showed reasonably appropriate frictional performance with moderate stability coefficient (α) and variability coefficient (γ). Hence, composites for the friction braking applications may optimally be best designed with the combined incorporation of ceramic whiskers, ceramic fibers, and aramid fiber although for developing friction materials with enhanced friction stabilization and to counter wear via the formation of a stable friction film has reportedly been recommended in the literature.[29]

Interdependence of fade-recovery-temperature rise of the disc

The enahncement in fade and recovery performance of the composites is clearly shown in Figure 3(d). The fade performance deemed to be satisfactory for the composites having ceramic fiber/whiskers = 13.75 wt % each, in complementary combination with aramid fiber = 2.5 wt % (i.e., TSC-1,TSC-2) whereas, it deteriorates (>58%) strongly for the composites having ceramic whiskers/fiber <13.75 wt % each in complementary combination with aramid fiber >2.5 wt % (i.e., TSC-3, TSC-4, and TSC-5). In general, μ-fade performance of such composites deteriorates with stepwise decrement in wt % of ceramic fiber/whiskers and complementary increment in wt % of organic fiber. The detoriated fading peformance attributed to the presence of organic natured aramid fiber and step-wise increment in its content that facilitates the formation of a stable load-carrying friction film at elevated temperatures with a shear thinning interfacial rheology that enabling the contact patches to become more lubricating without much reduction in the surface hardness of the composites may be conjectured. However, recovery performance has been observed to exceed 100% irrespective of the fiber/whisker combinations. The recovery remained comparable for the composites TSC-1, TSC-2, and TSC-3 while an abrupt increase of $\sim$ 20% is observed from TSC-3 to TSC-4 followed by a nominal decrease in recovery for TSC-5. Such a behavior may be attributed to the formation-deformation-damage-reformation dynamics of the operating friction film at the braking junction/interface, which is facilitated by the presence of aramid. The μ-recovery is restored due to the disintegration of the loosely attached wear debris from the secondary contact patches, which facilitate the process of rolling abrasion as they become hardened with the cooling down of the braking interface. The mechanism of fade and recovery in brake composites has also been reported in our earlier articles.[25,27–29] It must be mentioned that fade in the range 0–30% and recovery in the range 90–140% is typically desirable for brake friction composites as per IS 2742.

The vicious interdependence of fade-recovery-wear-temperature rise of the disc has already been discussed in literature.[28,29] As the disc temperature rise (DTR) drops across the composition variations, recovery, and wear performance improves whereas fade performance deteriorates as shown in Figure 3(a–g). A quantitative semi-empirical performance-composition-domain correlation thematic diagram (Table IV) may be useful to depict such interdependence and is already discussed in the literature pertaining to friction material based on potassium titanate whiskers in combination with aramid fibers[28] and alumino-silicate fibers in combination with aramid fiber.[29] The overall performance of the investigated composites can be categorized into three levels based on the proximity of the performance defining attributes (fade, recovery, braking induced temperature rise of the disc, and wear), where the standard deviation in the proximity level remained within the range of 5–10%. Thus, composite TSC-1 forms the domain-I while composites TSC-2 and TSC-3 form the domain-II. In the sequence TSC-4 and TSC-5 form the domain-III. The performance-defining attribute, the maximum DTR suffers a decrease of $\sim$ 74°C across the domain-I to domain-II and 39°C across the domain-II to domain-III within the investigated set of composites. Such a gradual decrease in temperature rise of the disc across the composition domain has been observed to be in close correspondence to an increase of $\sim$ 35% in the extent of fade across the domain-I to domain-II and $\sim$ 26% across the domain-II to domain-III. However, a nominal

TABLE IV
Composition-Domain Performance-Attribute Correlation Thematic Diagram

Composition domain	Performance attributes			
	Friction fade (%)	Friction recovery (%)	Disc temperature rise (°C)	Wear (g)
Domain –I (TSC-1)	13.73 TSC-1; (abs.)	113.47 TSC-1; (abs.)	525 TSC-1; (abs.)	4.35 TSC-1; (abs.)
Domain –II (TSC-2,TSC-3)	~ 35%[a]	~ 1.2%[b]	−73.5°C[c]	~ 61.5% decrease; ~ 2.7 g decrease
	38.75 TSC-2; 58.36 TSC-3; {48.56} avg.	113.39 TSC-2; 115.92 TSC-3; {114.66} avg.	448 TSC-2; 455 TSC-3; {451.5 ± 3.5} avg.	1.60 TSC-2; 1.75 TSC-3; {1.675} avg.
Domain-III (TSC-4,TSC-5)	~ 26%[a]	~ 19.3%[b]	−39°C[c]	~ 8.95% decrease ~ 0.15 g decrease
	74.14 TSC-4; 75.43 TSC-5; {74.79} avg.	136.14 TSC-4; 131.79 TSC-5; {133.97} avg.	400 TSC-4; 425 TSC-5; {412.5 ± 12.5}avg.	1.60 TSC-4; 1.45 TSC-5; {1.525} avg.

[a] Quantitative appreciation across the composition domains in friction fade.
[b] Quantitative changes across the composition domains in friction recovery.
[c] Quantitative reduction in the DTR across the composition domains.
Subscript-Abs.: Absolute value of the performance attribute when there is only one composition as in domain-I.
Subscript-Avg.: Average of the performance attribute of the two compositions in each domain (domain-II and III).

increase of ~ 1.2% in the extent of recovery has been observed across the domain-I to domain-II and an increase of ~ 19.3% has been observed across the domain-II to domain-III. Thus, fade-recovery-temperature rise of the disc are inherently observed to be composition domain dependent. The lowest amount of fade inspite of very high DTR may be attributed to the higher weight fraction of potassium titanate whiskers and ceramic fibers that helps in arresting/minimizing thermally induced friction decay effect because of their excellent thermo-mechanical properties, good abrasive nature due to higher Moh's hardness and higher adiabatic potential than that of aramid fiber. Thus fiber-combinations enhance the abrasive component relative to adhesive component in determining the overall performance. However, highest extent of fade with the lowest DTR is attributed to the fact that higher proportion of aramid fiber are responsible for enhancing the shear thinning behaviour of the operating friction-film/tribo-layer at the braking junction that minimizes the abrasive component of friction by maximizing the adhesive contribution. Mechanistically, the distinct transition across the domains may well be in correspondence with a transition from friction film hardening (due to higher adiabatic potential ceramic ingredients) with braking instances to shear thinning rheology of the friction film (due to aramid fiber). Similarly, it is observed that as the temperature rise of the disc across the composition domain decreases; the wear of the composites decreases and the extent of decrease is ~ 61.5% (~ 2.7 g) across the domain-I to domain-II and ~ 8.95% (~ 0.15 g) across the domain-II to domain-III. Such composition dependent wear transitions may be thermally activated though adherence of friction-film/tribo-layer with two rubbing halves may lead to wear minimization/stabilization of such composites. This investigation thus comprehensively demonstrates the performance-composition-domain correlation thematic diagram establishing the possible interrelations between the various performance-defining attributes of the brake composites.

Wear performance of the composite

The maximum temperature rise of the disc and the wear performance of the composites (in terms of weight loss and pad thickness loss) is shown in Figure 3(e–g). The resemblance of the trend of wear performance of composites and rise in disc temperature indicates that wear mechanism of these composites is largely thermally activated. This may be attributed to the characteristically abrasive nature of alumino-silicate fiber and potassium titanate whiskers. It is well understood that a higher wear is undesirable as it may eventually cause disc thickness variations (DTV) and therefore noise, vibration, and judder propensity. Such undesirable phenomenon may be arrested by appropriately designing the volumetric loading and selection of the fibers. Interestingly, wear decreases by ~ 63% with the initial addition of the aramid fibers in the composition range of TSC-1 to TSC-2. It was observed that as aramid content increased wear tended to be stabilized. This may have been promoted by the aramid fiber enhancing the lubricating action and adhesive contribution over abrasive that ultimately reduced wear.

Analysis of friction and wear performance of the composites

Analysis of μ-performance has been carried out by following an empirical assumption that the friction performance tends to abide by the linear polynomial approach where μ-performance (μ_p) is considered to

be a functional variable of the combination of μ-static (μ_s), μ-fade (μ_f), μ-recovery (μ_r), and frictional fluctuations ($\Delta\mu = \mu_{max} - \mu_{min}$) while the other parameters remain constant. Mathematically, such a relationship may be stated as[25,26,28–29]:

$$\mu_p = K + a\ \mu_s + b\ \mu_f + c\ \mu_r + d\ (\Delta\mu) \quad (3)$$

where, *K, a, b, c,* and *d* are the coefficients of material contribution, μ-static, μ-fade, μ-recovery, and frictional–fluctuations, respectively. On substituting the corresponding values for each composition, the five equations that evolve are,

$$0.368 = K + 0.413\ a + 0.333\ b + 0.438\ c + 0.519\ d \quad (4)$$

$$0.351 = K + 0.350\ a + 0.215\ b + 0.398\ c + 0.473\ d \quad (5)$$

$$0.377 = K + 0.353\ a + 0.157\ b + 0.437\ c + 0.463\ d \quad (6)$$

$$0.321 = K + 0.296\ a + 0.083\ b + 0.437\ c + 0.419\ d \quad (7)$$

$$0.346 = K + 0.302\ a + 0.085\ b + 0.456\ c + 0.444\ d \quad (8)$$

On solving the above equations [i.e., eqs. (4–8)], the values of the coefficients may be obtained as $K = 0.2561$, $a = 2.3510$, $b = -0.6131$, $c = -0.6162$, and $d = -0.7148$. This evident that the static friction factor dominates inherent material factor in controlling the μ-performance. However, fade factor, recovery factor, and fluctuation factor seems to counterbalance the contribution of static friction and inherent material factor under the above stated assumptions.

The wear analysis has been carried out following the eq. (9), between the wear of the friction materials in terms of weight loss (ΔW) and wear factor (K), load (F), sliding speed (V), and braking time (t) where *a, b,* and *c* are the coefficients corresponding to load, speed, and braking duration for a given braking system.[32] The equation may be given as,

$$\Delta W = K\ \times F^a\ \times V^b\ \times t^c \quad (9)$$

Wear of the material and the mean temperature of the surface found to be varying nonlinearly as a function of braking pressure and sliding speed. Hence, an empirical relation, that is, eq. (10) resembling the Rhee equation correlating the wear and the friction decay, friction build-up and maximum DTR has been adopted to analyze the wear performance. It is assumed that the contribution of braking pressure and sliding speed is reflected in the temperature rise of the disc and the contribution of the static friction in wear is assumed negligible.

$$\Delta W = K_o\ \times \mu_f^{k1}\ \times \mu_r^{k2}\ \times T^{k3} \quad (10)$$

where ΔW is the weight loss and K_o, k_1, k_2, and k_3 are the inherent material contribution to wear, fade-coefficient, recovery-coefficient, and temperature-coefficient. On simplifying, the equation reduces to,

$$\log \Delta W = \log K_o\ + k_1 \log \mu_f + k_2 \log \mu_r + \ k_3 \log T \quad (11)$$

On substituting the values we get,

$$\log 4.35 = \log K_o + k_1 \log 0.333 + k_2 \log 0.438 + k_3 \log 798.0 \quad (12)$$

$$\log 1.60 = \log K_o + k_1 \log 0.215 + k_2 \log 0.398 + k_3 \log 720.5 \quad (13)$$

$$\log 1.75 = \log K_o + k_1 \log 0.157 + k_2 \log 0.437 + k_3 \log 728.0 \quad (14)$$

$$\log 1.60 = \log K_o + k_1 \log 0.083 + k_2 \log 0.437 + K_3 \log 673.0 \quad (15)$$

$$\log 1.45 = \log K_o + k_1 \log 0.085 + k_2 \log 0.456 + k_3 \log 698.0 \quad (16)$$

On solving the eqs. (12–16), the various coefficients may be obtained as; $K_o = 186.65$, $k_1 = 3.73$, $k_2 = 18.89$, and $k_3 = -24.78$. This indicates that the inherent material contribution and the contribution from fade and recovery predominate the temperature rise of the disc in determining the wear behavior of such composites. Further, it is also observed that the material coefficient and the coefficient due to DTR tend to abate each other appreciably. Thus, it may be reiterated that wear of these composites may be largely thermally activated.

WORN SURFACE MORPHOLOGY STUDIES

An observation into the section perpendicular to the surface of the pad reveals distinct three layers under low magnification optical microscope. Macroscopically, the top layer, that is, the sliding surface consists of dark layer ~ 1–2 mm thick; comprises of the reaction products formed due to intense frictional heat across the sliding interface. Bottom most layer of ~ 7–10 mm thick comprises of bulk material and the middle most layer of ~ 1–2.5 mm is known as heat affected sub-surface zone.

In general, worn surface micrographs of the composites as shown in Figure 4(a–e) reveals distinct characteristics of friction film/contact patch/wear debris formation and inter-mixing of the fibrous and powdery/particulate constituents. Appearance of transverse cracks, conjectured to be due to thermally induced fatigue, on the surface facilitates pits formation, compaction fine wear debris leading to loosely adhering secondary patches, and crack nucleation/propagation have been construed as typical

characteristics of the worn surface morphology and as the factors responsible for subsurface damage/degradation in braking situations. The magnified view clearly reveals protruded fibers and other ingredients from the bulk of the material while nano-structured friction-film formation on the top of the surface covering the underlying materials may be responsible for lower wear, reduced friction fluctuations, and stabilization of μ-performance.

The micrograph corresponding to TSC-1 shown in Figure 4(a) revealed the presence of wear pits due to dislodged ingredients, formation of stable contact patches due to compaction of wear debris and exposed ceramic fibers and whiskers on the worn surface. Further, the worn surface distinctly reveals the loosely adhered secondary contact patches to the subsurface. The thickness of the contact patch remained in the range of $\sim$ 0.1–1 μm. The large fade resistance and low variability coefficient the composite TSC-1 may be attributed to the combined role of exposed hard ceramic fibers/whiskers in combination with adequate amount of secondary friction contact patches. In the composite TSC-2, the worn surface reveals presence of both adhesive and abrasive components of wear as reveled from the fibrous nature of the exposed friction surface and the secondary contact patches [Fig. 4(b)]. The simultaneous presence of ceramic fibers and whiskers in combination with aramid fibers has led to the generation of friction contact patches with intensely abraded/slid alumino-silicate fibers and whiskers. In contrast, in TSC-3 showing the maximum friction stability coefficient has shown worn surface, morphology characterized by thermally activated surface microcracks, wear pits with embedded fibers/whiskers, and random spatial distribution of the fibrous ingredients giving rise to an isotropic/stable frictional response [Fig. 4(c)]. The similarity in the wear surface morphology of TSC-1, TSC-2, and TSC-3 has also been reflected in their comparable recovery performances. In contrast, composites TSC-4 and TSC-5 the absence of exposed ceramic fibers/whiskers and surface undulations due to the absence of wear pits indicate that the friction mechanism is largely dominated by adhesive contribution, which typically cause a higher recovery response and much less wear [Fig. 4(d,e)]. Understandably, the higher amount of aramid content in these composites may be responsible for wear reduction and enhancement in recovery performance.

CONCLUSIONS

The brake pad friction material based on ternary combination of potassium titanate whiskers, ceramic (alumino-silicate) fiber, and aramid fiber were designed and fabricated. The physical and mechanical properties have been found to be well within the industrial norms. The frictional response clearly revealed three distinct modes of friction evolution (viz., friction-build up, friction-peaking, and friction-decay) irrespective of the compositional variations and test runs (viz., cold, fade, and recovery runs). Broadly, the friction coefficients remained in the range of $\sim$ 0.3–0.5. The composite having more ceramic whiskers/fiber content (=13.75 wt % each) in combination with less aramid fiber (=2.5 wt %) showed promising friction coefficients as well as much less fading tendency. The composite with 7.5 wt % of aramid fiber showed maximum friction stability whereas the frictional amplitude ($\mu_{max} - \mu_{min}$) remained lowest in the composites with least ceramic content and maximum aramid fibers (=10 wt %). From fade-resistance point of view high alumino-silicate fiber and whiskers in combination with low aramid content proved to be synergistic. The recovery performance remained above 100% irrespective of the composition variables. The stability coefficient (α) remained moderate whereas variability coefficient (γ) showed increasing trend with increase in aramid content due to its shear thinning rheology of the friction film. Overall, the composites for the friction braking applications may optimally be best designed with the combined incorporation of whiskers, ceramic fiber, and aramid fiber proportions of 13.75 : 13.75 : 2.5, although wear remained a concern for the said composite. A semi-empirical "composition-domain performance-attribute" thematic correlation diagram is established to analyze interdependence of fade, recovery, DTR, and wear characteristics. Analysis of friction and wear data has revealed the predominance of inherent material contribution and the contribution from fade and recovery whereas wear remained mostly thermally activated. Worn surface morphology revealed the underlying role of the generation of wear pits, contact patches, and exposed fibrous ingredients in controlling the tribo-performance of the developed hybrid composites.

NOMENCLATURE

μ-performance (μ_p)	The average of COF taken after 1 s for the fade and recovery runs at temperature greater than 100°C.
μ-fade (μ_f)	The minimum COF for the fade run taken after 270°C.
% Fade	The ratio of difference of (μ-performance and μ-fade) to μ-performance.
μ-Recovery (μ_r)	The maximum COF for the recovery run taken after 100°C.

% Recovery	The ratio of μ-recovery to μ-performance.
μ_{max}	The highest COF for the cold, fade, and recovery runs.
μ_{min}	The lowest COF for the cold, fade, and recovery runs.
Stability coefficient (α)	The ratio of μ-performance to μ_{max}.
Variability coefficient (γ)	The ratio of μ_{min} to μ_{max}.

Authors gratefully acknowledge Allied-Nippon Industries Limited, Sahibabad, U.P, India, for extending their facilities to carry out a part of this research work.

References

1. Bijwe, J. Polym Compos 1997, 18, 378.
2. Hoyer, L. G.; Bach, A.; Nielsen, G. T.; Morgen, P. Wear 1999, 232, 168.
3. Liu, T.; Rhee, S. K.; Lawson, K. L. Wear 1980, 60, 1.
4. Starczewski, L.; Szumniak, J. Polymeric Compos Metal Surface Coat Tech 1998, 100, 33.
5. Eriksson, M.; Bergman, F.; Jacobson, S. Wear 2002, 252, 26.
6. Ostermeyer, G. P.; Muller, M. Tribol Int 2006, 39, 370.
7. Osterle, W.; Dorfel, I.; Prietzel, C.; Rooch, H.; Blulthe, A. L. C.; Degallaix, G.; Desplanques, Y. Wear 2009, 267, 781.
8. Filip, P.; Weiss, Z.; Rafaja, D. Wear 2002, 252, 189.
9. Cho, M. H.; Cho, K. H.; Kim, S. J.; Kim, D. H.; Jang, H. Tribol Lett 2005, 20, 101.
10. Satapathy, B. K.; Bijwe, J. Wear 2004, 257, 573.
11. Satapathy, B. K.; Bijwe, J. Compos A 2006, 37, 1557.
12. Halberstadt, M. L.; Rhee, S. K.; Mansfield, J. A. Wear 1978, 46, 109.
13. Kim, S. J.; Jang, H. Tribol Int 2000, 33, 477.
14. Gopal, P.; Dharani, L. R.; Blum, F. D. Wear 1996, 193, 199.
15. Gopal, P.; Dharani, L. R.; Blum, F. D. Wear 1996, 193, 180.
16. Sampath, V. Mater Manufacturing processes 2006, 21, 47.
17. Kim, S. J.; Cho, M. H.; Lim, D. S.; Jang, H. Wear 2001, 251, 1484.
18. Kim, S. J.; Cho, K. H.; Bash, R. H.; Fash, J. W.; Jang, H. Tribol Lett 2004, 17, 655.
19. Cho, K. H.; Cho, M. H.; Kim, S. J.; Jang, H. Tribol Lett 2008, 32, 59.
20. Cho, M. H.; Kim, S. J.; Kim, D.; Jang, H. Wear 2005, 258, 1682.
21. Kim, Y. C.; Cho, M. H.; Kim, S. J.; Jang, H. Wear 2008, 264, 204.
22. Liwen, M. U.; Feng, X.; Zhu, J.; Wang, H.; Sun, Q.; Shi, Y.; LU, X. Tribol Trans 2010, 53, 189.
23. Ozturk, B.; Arslan, F.; Ozturk, S. Tribol Int 2007, 40, 37.
24. Han, Ye.; Tian, X.; Yin, Y. Tribol Trans 2008, 51, 779.
25. Dakar, N.; Tomar, B. S.; Satapathy, B. K.; Patnaik, A. Mater Des 2010, 31, 723.
26. Dakar, N.; Tomar, B. S.; Satapathy, B. K. Mater Des 2009, 30, 4369.
27. Satapathy, B. K.; Bijwe, J. J. Reinf Plast Compos 2005, 24, 563.
28. Kumar, M.; Satapathy, B. K.; Patnaik, A.; Kolluri, D. K.; Tomar, B. S. Tribol Int 2011, 44, 359.
29. Patnaik, A.; Kumar, M.; Satapathy, B. K.; Tomar, B. S. Wear 2010, 269, 891.
30. Mahapatra, S. S.; Patnaik, A. Mater Des 2009, 30, 2791.
31. Replacement brake lining assemblies. ECE regulation no. 90, Inter Europe regulation limited 1997. UN 31 March, 1993.
32. Rhee, S. K. Wear 1970, 16, 431.